Supporting Information

Tuning the Microenvironment in Gas-Diffusion Electrodes Enables High-Rate CO_2 Electrolysis to Formate

Zhuo Xing,[1,2] Xun Hu,[1]* and Xiaofeng Feng[2,3]*

[1]School of Material Science and Engineering, University of Jinan, Jinan 250022, China

[2]Department of Physics, University of Central Florida, Orlando, Florida 32816, United States

[3]Renewable Energy and Chemical Transformations (REACT) Cluster, University of Central Florida, Orlando, Florida 32816, United States

*E-mail: mse_hux@ujn.edu.cn (X.H.); Xiaofeng.Feng@ucf.edu (X.F.)

This PDF file includes Experimental Methods, Figures S1−S13, Table S1, and References.

Experimental Methods

(1) Chemicals

Cetyltrimethylammonium bromide (CTAB), Bismuth nitrate pentahydrate ($Bi(NO_3)_2{\cdot}5H_2O$, 98%), urea, ethanol, isopropanol (Certified ACS), sulfuric acid (H_2SO_4, 98%), hydrogen peroxide (H_2O_2, 30%, Certified ACS), potassium hydroxide (KOH, 99.98%), dimethyl sulfoxide (Certified ACS), and deuterium oxide (D_2O, for NMR, 99.8 atom% D) were purchased from Fisher Scientific. Vulcan XC-72 carbon black, AvCarb GDS2230 carbon substrates, Nafion 1110 membranes were purchased from Fuel Cell Store. Nafion perfluorinated resin solution (5 wt%) was purchased from Sigma-Aldrich. PTFE nanopowder (APS 30−40 nm) was purchased from Nanoshel LLC. Leak-free Ag/AgCl reference electrodes (Model LF-1) were purchased from Harvard Apparatus. CO_2 (99.999%), Ar (99.999%), and H_2 (99.999%) gases were purchased from Airgas. Deionized water with a specific resistance of 18.2 MΩ·cm was used throughout the experiments.

(2) Preparation of BiOON Catalyst

BiOON catalyst was synthesized by hydrothermal method with cetyltrimethylammonium bromide (CTAB) as a surfactant.[1] Typically, 970 mg of $Bi(NO_3)_2{\cdot}5H_2O$ was dissolved in 60 mL of water, followed by the addition of 500 mg of CTAB. Then, a urea-ethanol solution was prepared by adding 3.0 g of urea to 40 mL of ethanol followed by sonication. Next, the urea-ethanol solution was quickly added to the $Bi(NO_3)_2$ aqueous solution and stirred for 30 min to form a homogeneous solution, which was subsequently kept at 90 °C in a water bath for 4 h. White powder of BiOON was collected after centrifugation, washing with water and ethanol, and drying at 60 °C.

(3) Physical Characterizations

Transmission electron microscopy (TEM) images were acquired by a FEI Tecnai F30 transmission electron microscope with a field emission gun operated at 200 kV. Scanning electron microscopy (SEM) images and energy-dispersive X-ray spectroscopy (EDS) mapping were acquired using a ZEISS Ultra-55 FEG scanning electron microscope. X-ray diffraction (XRD) patterns were collected by a PANalytical Empyrean diffractometer with a 1.8 KW copper X-ray tube. *Operando* X-ray absorption spectroscopy (XAS) characterization was performed at the Beamline 2-2 of the Stanford Synchrotron Radiation Lightsource using a modified H-cell and fluorescence yield mode, and XAS data were processed using the ATHENA software.[2] Contact angles were measured using an Ossila L2004A1 Contact Angle Goniometer.

(4) Preparation of Working Electrodes

First, 12 mg of the synthesized BiOON powder and 12 mg of Vulcan XC-72 carbon black were each dispersed in 1 mL of isopropanol. Then, 3.1, 7.0, 12.0, 18.7, and 28.0 mg of PTFE nanopowder (APS 30−40nm, Nanoshel LLC) were each dispersed in 2 mL of isopropanol. After sonication for 1 h, the BiOON dispersion, carbon black dispersion, corresponding PTFE dispersion, and 100 μL of Nafion solution (5 wt%) were mixed and sonicated for another 1 h, which were used as catalyst inks with a PTFE mass ratio of 10%, 20%, 30%, 40%, and 50%, respectively. Each catalyst ink was deposited on an AvCarb GDS2230 carbon substrate using a homemade XY plotter equipped with an airbrush. All samples were dried overnight before testing. The loading of BiOON catalyst on one electrode was around 0.65 ± 0.05 mg cm^{-2}.

(5) Electrochemical Measurements

CO_2 electrolysis was performed using a home-built flow cell with gas-diffusion electrodes (GDEs), as schematically illustrated in Figure S3, which consists of a Ti current collector with gas-diffusion channels, cathodic GDE with catalyst layer on AvCarb GDS2230 substrate, a 3D-printed chamber with ports for electrolyte flow and reference electrode, and an Fe-Ni foam inserted in a pocket of another Ti current collector as the anode.[3] The gas-diffusion channels have an interdigitated design with a depth of 0.20 mm and a density of 50 channels cm^{-1}. The above prepared electrodes were used as cathodes, and a leak-free Ag/AgCl electrode (Harvard Apparatus, Model LF-1) was used as reference electrode. A piece of Nafion 1110 membrane was used to separate the cathode and the anode chambers. The catholyte and the anolyte were each 20 mL of 1 M KOH solution, circulated using peristaltic pumps at a flow rate of 2.0 mL min^{-1}. CO_2 gas was supplied to the GDE cell by an Alicat mass flow controller at a flow rate ranging from 3−15 sccm. Controlled potential electrolysis was performed by a Gamry Interface 1000 potentiostat, and the applied potentials were iR-compensated using the Current Interrupt mode. All potentials are reported with respect to the reversible hydrogen electrode (RHE) in this work. The reported current densities were normalized to the effective geometric area of cathodes (0.66 cm^2). Gas-phase products of the electrolysis were quantified by periodic gas chromatography every 15 min using Ar carrier gas (SRI Multiple Gas Analyzer #5 equipped with molecular sieve 5A and HayeSep D columns). Solution-phase products were analyzed by nuclear magnetic resonance (NMR) spectroscopy (Bruker Avance III 500 MHz) after 30-min electrolysis under specific conditions. Typically, 500 μL of post-electrolysis catholyte was collected and mixed with 100 μL of D_2O containing 100 ppm dimethyl sulfoxide (DMSO) as an internal standard. ^1H NMR spectra were acquired using water suppression mode.

(6) Calculations of CO_2RR Current Density and Faradaic Efficiency

The molar quantity of produced formate was quantified by NMR spectroscopy and then converted to charges by multiplying by 2*F*, where *F* is the Faraday constant. The charges corresponding to formate production were divided by the total charges of the electrolysis to determine its Faradaic efficiency. The partial current density of CO production was calculated from the GC peak area as follows:

$$j_{\mathrm{CO}} = \frac{\text{peak area}}{\alpha} \times \text{outlet flow rate} \times \frac{2Fp}{RT} \times (\text{electrode area})^{-1}$$

where α is a conversion factor based on calibration of the GC with a standard sample, *R* is the ideal gas constant, *p* and *T* are the pressure and temperature of the gas, and outlet flow rate is the gas flow rate at the outlet of the GDE cell.[4] The Faradaic efficiency for CO production was calculated by dividing j_{CO} by the total current density. The partial current density for CO_2RR (j_{CO2RR}) was calculated using the following equation:

$$j_{\mathrm{CO_2RR}} = \frac{I_{\mathrm{total}} \times (\mathrm{FE_{HCOO^-}} + \mathrm{FE_{CO}})}{\text{electrode area}}$$

where FE_{HCOO-} and FE_{CO} are the Faradaic efficiencies for $HCOO^-$ and CO production, respectively. The single-pass CO_2 conversion rate (CR) was calculated using the following equation:

$$\mathrm{CR} = \frac{I_{\mathrm{total}} \times (\mathrm{FE_{HCOO^-}} + \mathrm{FE_{CO}})}{2F} \times \frac{RT}{p} \times (\text{inlet flow rate})^{-1} \times 100\%$$

where inlet flow rate is the flow rate of CO_2 gas delivered into the GDE cell. The reported CO_2RR current densities, Faradaic efficiencies, conversion rates, and their error bars were calculated from the measurements on three separately prepared samples under the same conditions.

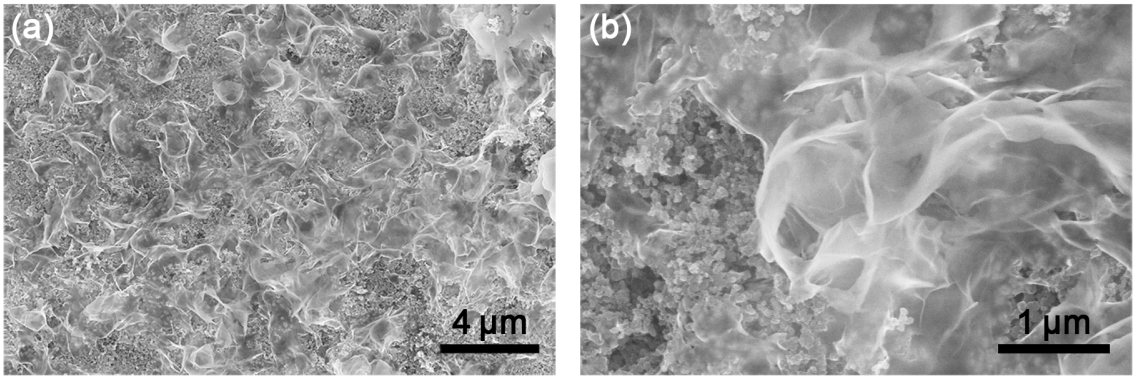

Figure S1. Top-view SEM images of the Bi/C electrode after CO_2 electrolysis.

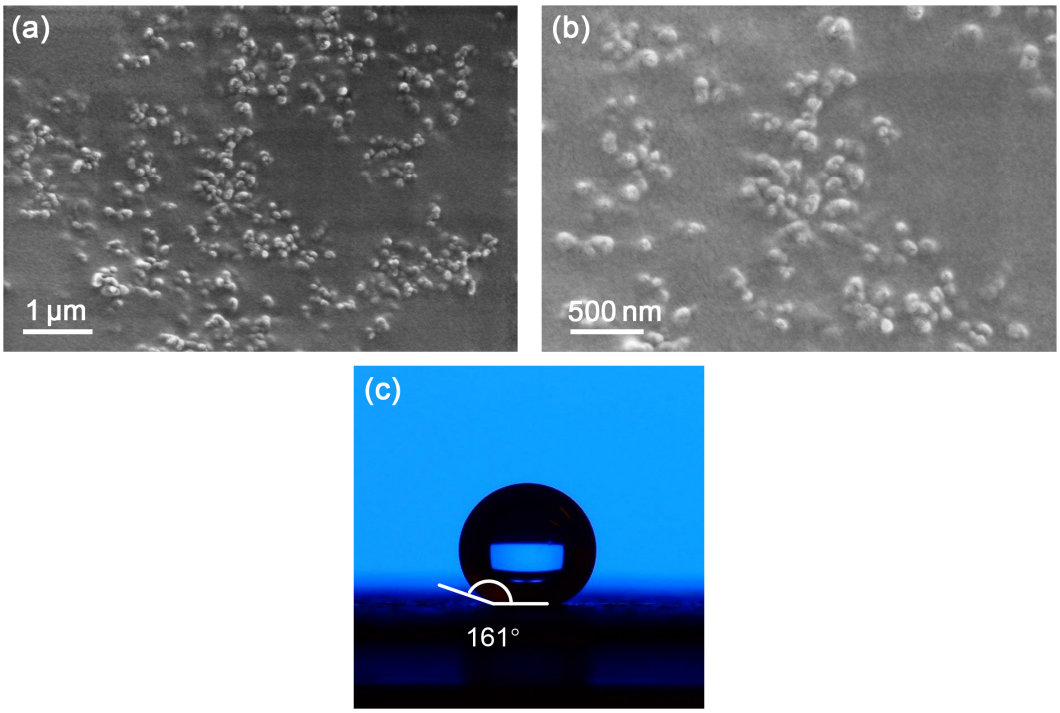

Figure S2. Characterization of the PTFE nanoparticles. (a−b) Typical SEM images acquired under low voltage (2 kV). (c) Contact angle measurement.

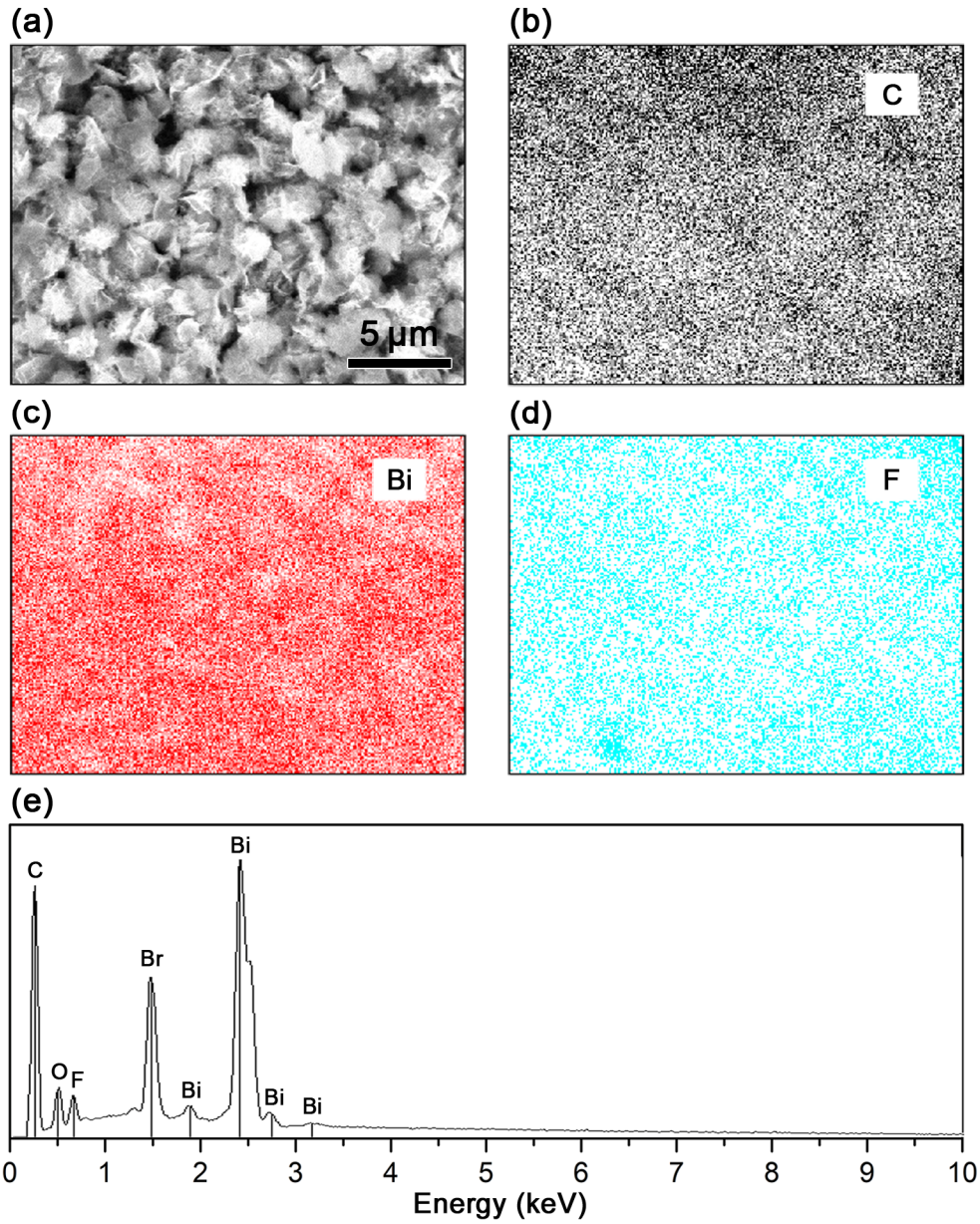

Figure S3. (a) Top-view SEM image of the Bi/C/30%PTFE electrode. (b−d) Energy-dispersive X-ray spectroscopy (EDS) mapping of C, Bi, and F elements in the area; and (e) corresponding EDS spectrum acquired in the area.

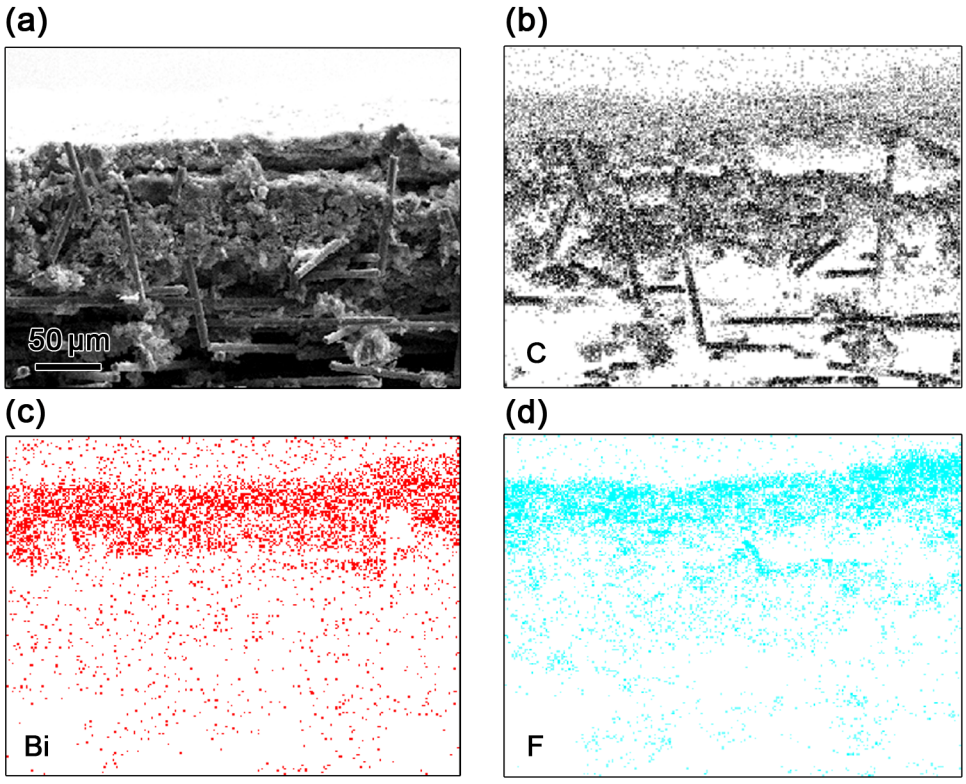

Figure S4. (a) Cross-sectional SEM image of the Bi/C/30%PTFE electrode. (b−d) Corresponding EDS mapping of C, Bi, and F elements in the area.

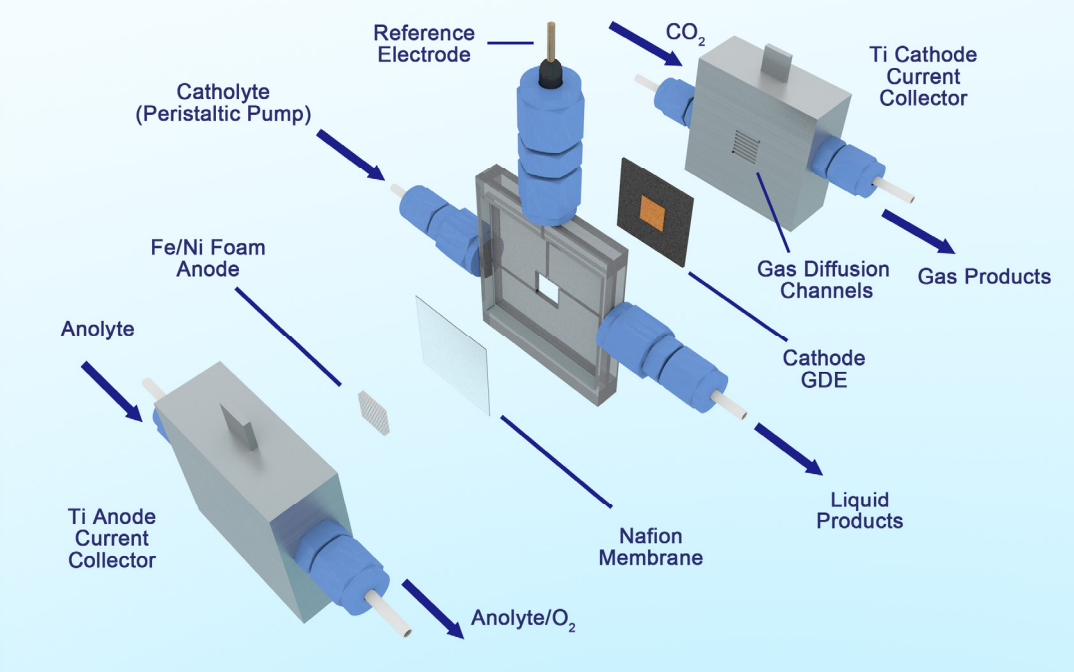

Figure S5. Schematic illustration of the configuration of the GDE flow cell for CO_2 electrolysis.

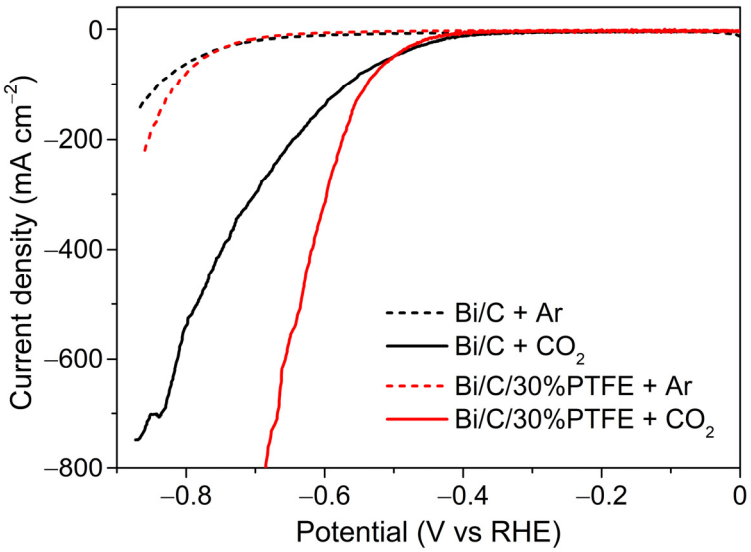

Figure S6. Linear sweep voltammetry (LSV) curves of the Bi/C and Bi/C/30%PTFE electrodes in 1 M KOH electrolyte under 6-sccm CO_2 or Ar gas flow. Scan rate: 10 mV s^{-1}.

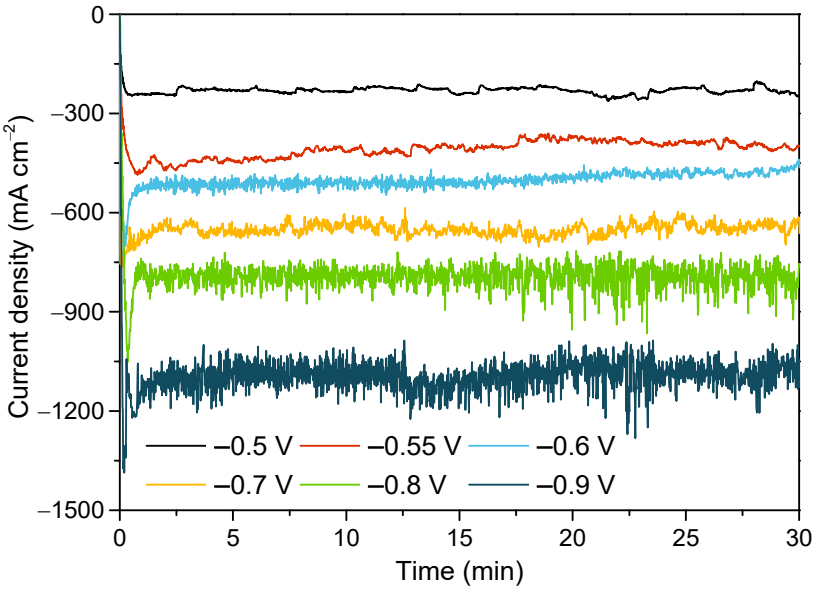

Figure S7. Representative chronoamperometric curves for CO_2 electrolysis on the Bi/C/30%PTFE electrode in the GDE flow cell with 1 M KOH electrolyte at various potentials.

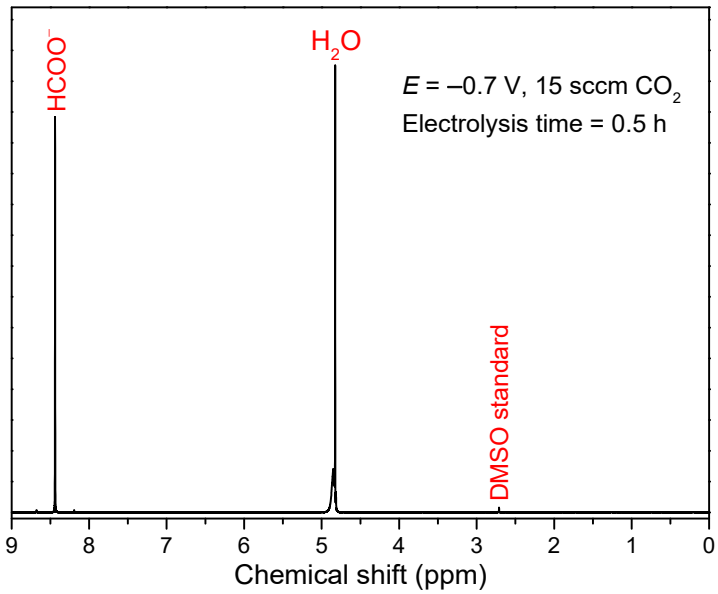

Figure S8. Representative NMR spectrum of the solution-phase product of the CO_2 electrolysis on the Bi/C/30%PTFE electrode.

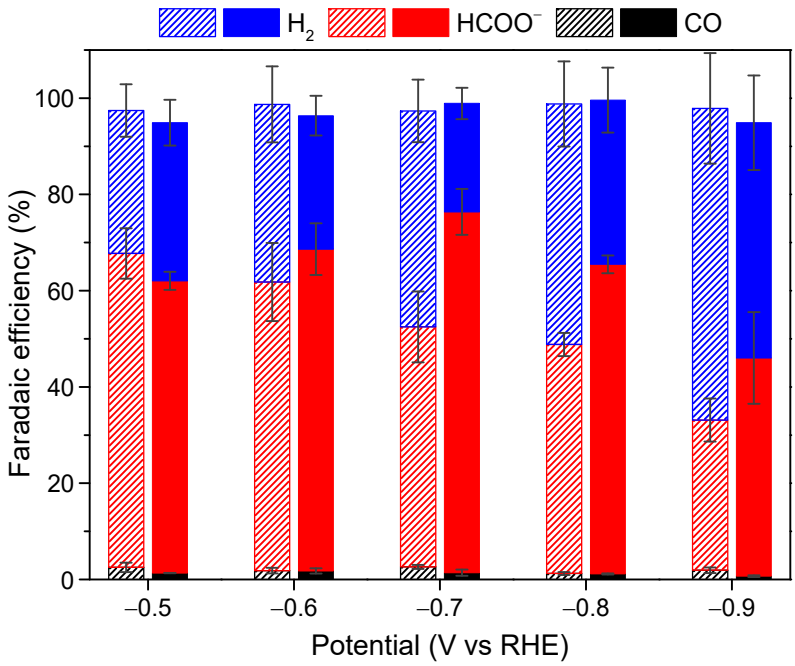

Figure S9. Faradaic efficiencies for CO_2RR on the Bi/C and Bi/C/30%PTFE electrodes at various potentials under 6 sccm CO_2 gas flow. The left column with pattern at each potential is for the Bi/C electrode, and the right column with no pattern is for the Bi/C/30%PTFE electrode.

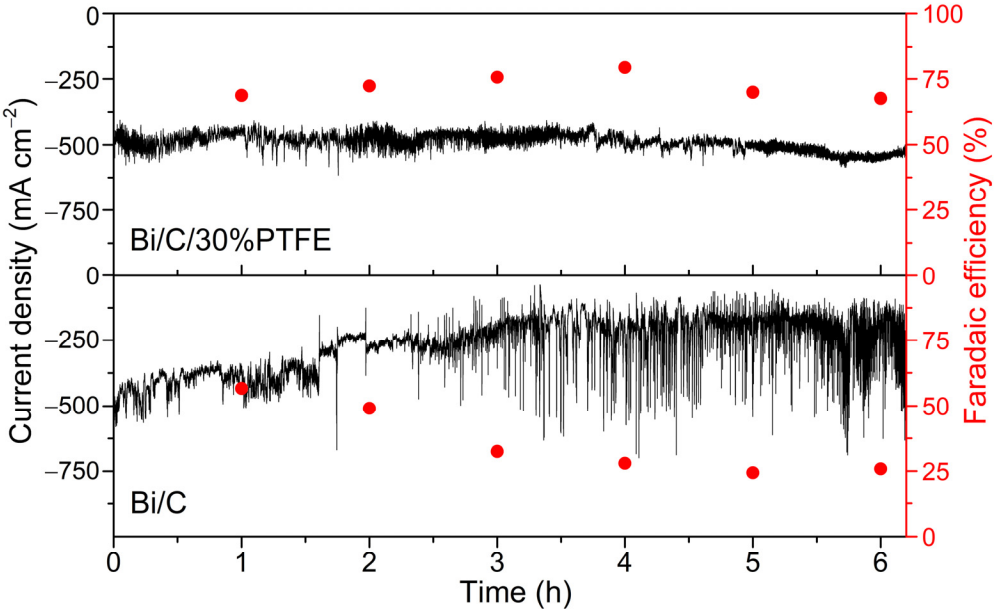

Figure S10. Comparison of the stability of the Bi/C and Bi/C/30%PTFE electrodes for CO_2RR at −0.6 V vs RHE under 6-sccm CO_2 gas flow in the GDE flow cell. The left axis (black) is the total current density, and the right axis (red) is the Faradaic efficiency for formate production.

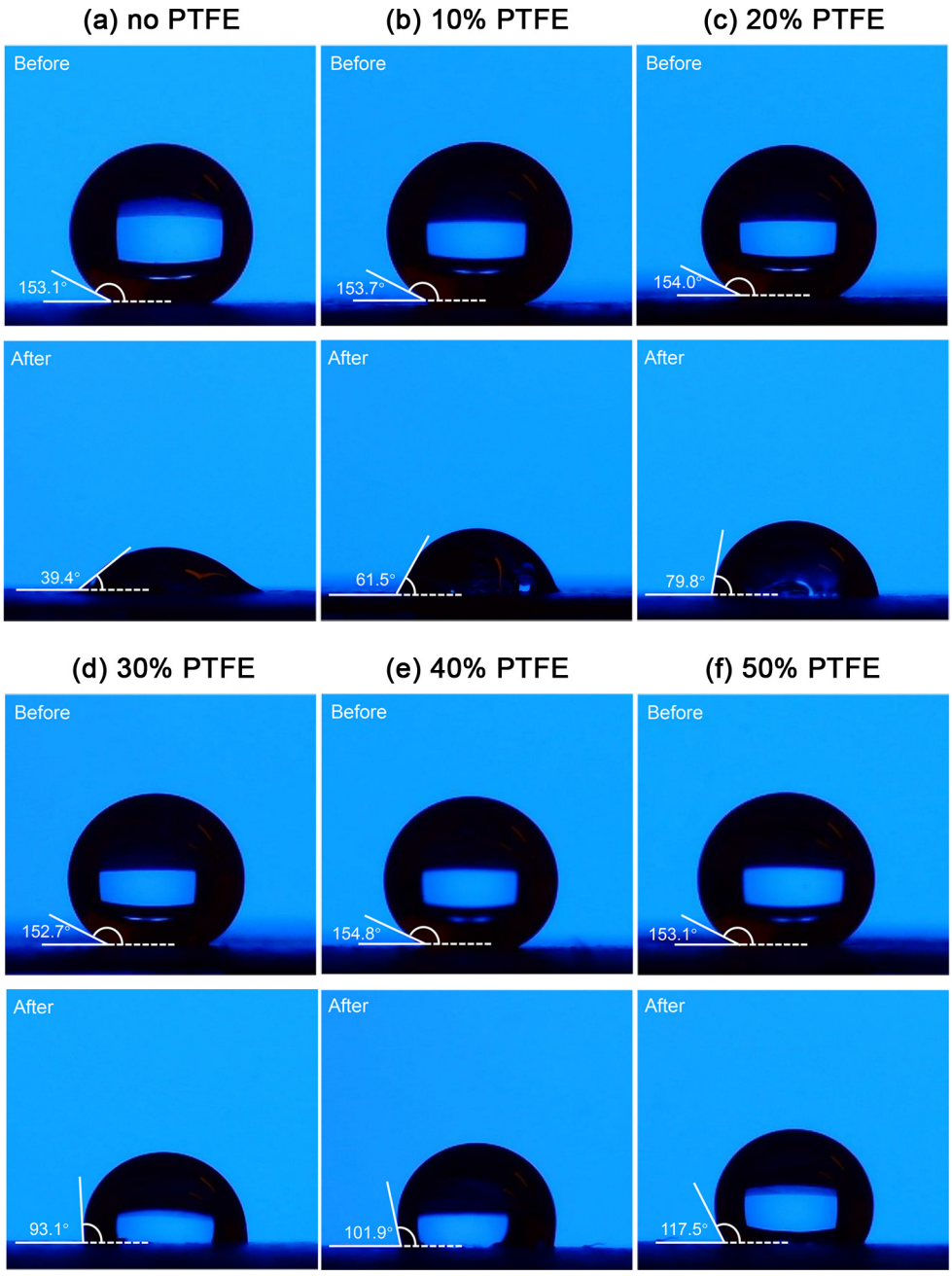

Figure S11. Contact angle measurements on the Bi-based electrodes with different PTFE loadings before and after CO_2 electrolysis at −0.7 V vs RHE in the GDE flow cell.

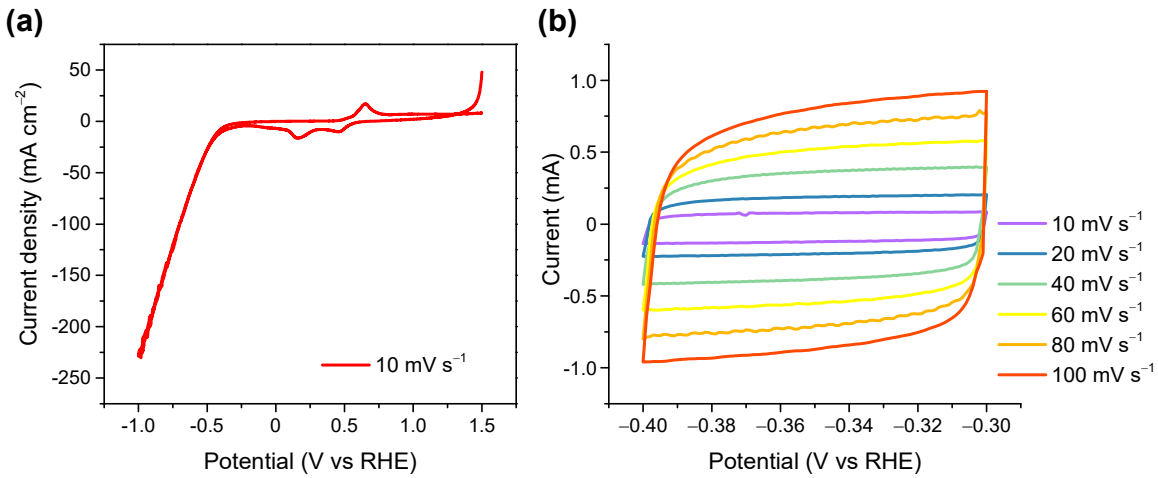

Figure S12. (a) Cyclic voltammogram (CV) acquired in a wide potential window at a scan rate of 10 mV s^{-1}. (b) CV scans measured in a narrow potential window where only double-layer charging and discharging occur at various scan rates.

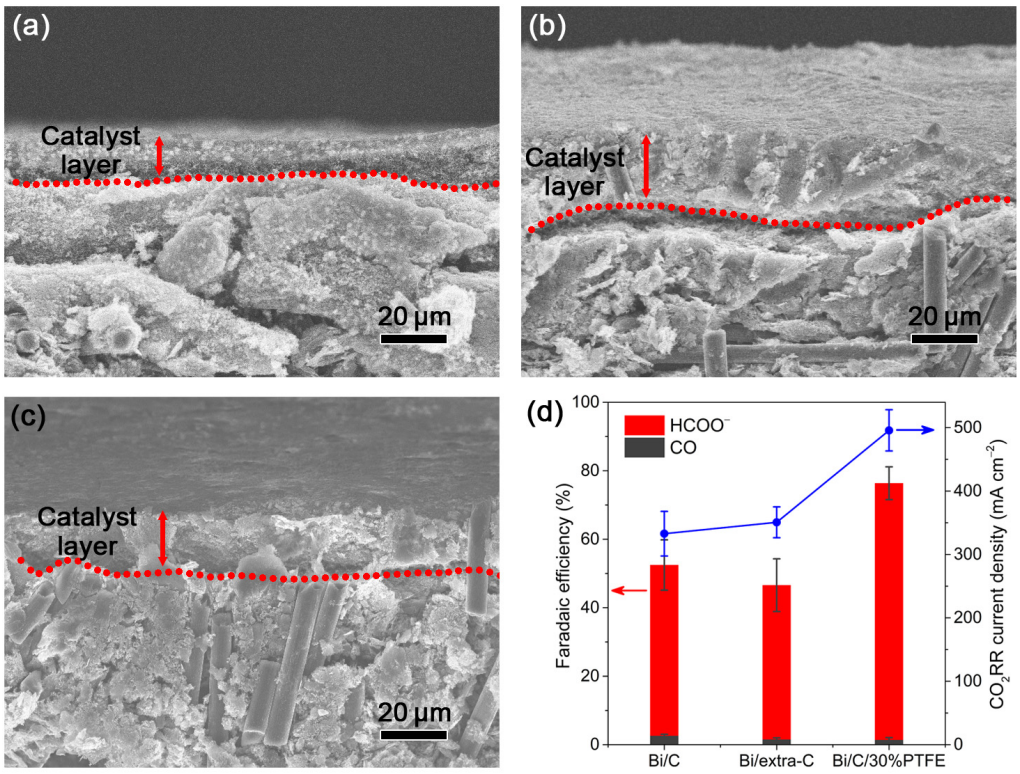

Figure S13. Comparative experiment to study the influence of the catalyst layer thickness. (a–c) Cross-sectional SEM images of the (a) Bi/C, (b) Bi/extra-C (with extra loading of carbon black), and (c) Bi/C/30%PTFE electrodes, where the boundary between the catalyst layer and the MPL is indicated by a dashed line. Their catalyst layer thicknesses were estimated to be: (a) 13.3 ± 2.4 μm, (b) 22.9 ± 1.9 μm, and (c) 18.6 ± 1.7 μm, respectively. (d) Faradaic efficiencies and partial current densities for CO_2RR on the three electrodes at −0.7 V vs RHE in the GDE flow cell. The error bars represent the standard deviation of three independent measurements.

Table S1. Summary of recently reported performance of CO_2RR to formate using GDE flow cells.

#	Catalyst	Catholyte	Applied potential (cathode or cell)	CO_2 gas flow rate (sccm)	FE_{CO2RR}	j_{CO2RR} (mA cm^{-2})	Electrode area (cm^2)	Single-pass conversion	Ref.
1	Bi flakes	1 M KOH	$E_{cathode}$ = −0.70 V_{RHE}	6	76%	496	0.66	38.0%	This work
				9	83%	677		34.6%	
				12	91%	686		26.3%	
2	2D-Bi nanosheets	2 M KOH	$E_{cathode}$ = −0.68 V_{RHE}	20	86.1%	185*	1	6.4%#	(1)
		solid electrolyte	E_{cell} = 2.81 V	20	82.7%	165.4	4	23.0%	
3	Bi nanosheets	0.5 M $KHCO_3$	$E_{cathode}$ = −0.98 V_{RHE}*	30	99%	54	1	1.3%#	(5)
4	Bi nanocrystals	3 M $KHCO_3$	E_{cell} = 6.97 V*	50	27%	108	4	6.0%#	(6)
5	Bi_2O_3 nanoparticles	1 M KOH	$E_{cathode}$ = −1.10 V_{RHE}	20	93%	208	1	7.2%#	(7)
6	Bi nanoparticles	1 M $KHCO_3$	$E_{cathode}$ = −1.05 V_{RHE}	50	92%	460	1	6.4%#	(8)
		solid electrolyte	E_{cell} = 2.19 V	50	95%*	440	4.75	29.1%#	
7	InP quantum dots	3 M KOH	$E_{cathode}$ = −2.6 V_{RHE}	50	93%	930	1	13.0%#	(9)
8	SnO_2 nanoparticles	1 M KOH	E_{cell} = 5.90 V	2000	90%	450	25	3.9%#	(10)
9	Sn_3O_4 nanosheets	1 M KOH	$E_{cathode}$ = −1.13 V_{RHE}	10	83.5%	465	1	32.4%#	(11)
10	SnO_2 nanoparticles	0.5 M Na_2SO_4 + 0.5 M Na_2CO_3	$E_{cathode}$ = −0.94 V_{RHE}	10	72%	385	0.25	6.7%#	(12)
11	Bi_2O_3 nanotubes	1 M KOH	$E_{cathode}$ = −0.58 V_{RHE}	20	98%	210	1	7.3%#	(13)

*These data were estimated from figures in the corresponding publications.

#The single-pass conversion rate (CR) was calculated using the following equation:

$$\mathrm{CR} = \frac{j_{\mathrm{CO2RR}} \times A}{2F} \times \frac{RT}{p} \times (\mathrm{CO_2\ flow\ rate})^{-1} \times 100\%$$

where j_{CO2RR} is the partial current density for CO_2RR, A is the geometric electrode area, F is the Faraday constant, R is the ideal gas constant, and T and p are the absolute temperature and pressure of the CO_2 gas.

References:

(1) Xia, C.; Zhu, P.; Jiang, Q.; Pan, Y.; Liang, W.; Stavitski, E.; Alshareef, H. N.; Wang, H. Continuous production of pure liquid fuel solutions via electrocatalytic CO_2 reduction using solid-electrolyte devices. *Nat. Energy* **2019**, *4*, 776−785.

(2) Ravel, B.; Newville, M. ATHENA, ARTEMIS, HEPHAESTUS: data analysis for X-ray absorption spectroscopy using IFEFFIT. *J. Synchrotron Radiat.* **2005**, *12*, 537−541.

(3) Ripatti, D. S.; Veltman, T. R.; Kanan, M. W. Carbon monoxide gas diffusion electrolysis that produces concentrated C_2 products with high single-pass conversion. *Joule* **2019**, *3*, 240−256.

(4) Ma, M.; Clark, E. L.; Therkildsen, K. T.; Dalsgaard, S.; Chorkendorff, I.; Seger, B. Insights into the carbon balance for CO_2 electroreduction on Cu using gas diffusion electrode reactor designs. *Energy Environ. Sci.* **2020**, *13*, 977−985.

(5) Yang, F.; Elnabawy, A. O.; Schimmenti, R.; Song, P.; Wang, J.; Peng, Z.; Yao, S.; Deng, R.; Song, S.; Lin, Y.; Mavrikakis, M.; Xu, W. Bismuthene for highly efficient carbon dioxide electroreduction reaction. *Nat. Commun.* **2020**, *11*, 1088.

(6) Li, T.; Lees, E. W.; Zhang, Z.; Berlinguette, C. P. Conversion of bicarbonate to formate in an electrochemical flow reactor. *ACS Energy Lett.* **2020**, *5*, 2624−2630.

(7) Deng, P.; Yang, F.; Wang, Z.; Chen, S.; Zhou, Y.; Zaman, S.; Xia, B. Y. Metal-organic framework-derived carbon nanorods encapsulating bismuth oxides for rapid and selective CO_2 electroreduction to formate. *Angew. Chem. Int. Ed.* **2020**, *59*, 10807−10813.

(8) Fan, L.; Xia, C.; Zhu, P.; Lu, Y.; Wang, H. Electrochemical CO_2 reduction to high-concentration pure formic acid solutions in an all-solid-state reactor. *Nat. Commun*. **2020**, *11*, 3633.

(9) Grigioni, I.; Sagar, L. K.; Li, Y. C.; Lee, G.; Yan, Y.; Bertens, K.; Miao, R. K.; Wang, X.; Abed, J.; Won, D. H.; García de Arquer, F. P.; Ip, A. H.; Sinton, D.; Sargent, E. H. CO_2 electroreduction to formate at a partial current density of 930 mA cm^{-2} with InP colloidal quantum dot derived catalysts. *ACS Energy Lett.* **2021**, *6*, 79−84.

(10) Chen, Y.; Vise, A.; Klein, W. E.; Cetinbas, F. C.; Myers, D. J.; Smith, W. A.; Deutsch, T. G.; Neyerlin, K. C. A robust, scalable platform for the electrochemical conversion of CO_2 to formate: Identifying pathways to higher energy efficiencies. *ACS Energy Lett.* **2020**, *5*, 1825−1833.

(11) Liu, L. X.; Zhou, Y.; Chang, Y. C.; Zhang, J.-R.; Jiang, L.-P.; Zhu, W.; Lin, Y. Tuning Sn_3O_4 for CO_2 reduction to formate with ultra-high current density. *Nano Energy* **2020**, *77*, 105296.

(12) Sen, S.; Brown, S. M.; Leonard, M.; Brushett, F. R. Electroreduction of carbon dioxide to formate at high current densities using tin and tin oxide gas diffusion electrodes. *J. Appl. Electrochem.* **2019**, *49*, 917−928.

(13) Gong, Q.; Ding, P.; Xu, M.; Zhu, X.; Wang, M.; Deng, J.; Ma, Q.; Han, N.; Zhu, Y.; Lu, J.; Feng, Z.; Li, Y.; Zhou, W.; Li, Y. Structural defects on converted bismuth oxide nanotubes enable highly active electrocatalysis of carbon dioxide reduction. *Nat. Commun.* **2019**, *10*, 2807.